

Design and fabrication of hollow out-of-plane silicon microneedles

Petr Jurčíček, Helin Zou, Shuiping Zhang, Chong Liu

Research Center for Micro System Technology (MST), Dalian University of Technology, Dalian, People's Republic of China
E-mail: zouhl@dlut.edu.cn

Published in Micro & Nano Letters; Received on 25th November 2012; Revised on 17th January 2013; Accepted on 18th January 2013

The design and fabrication of hollow out-of-plane silicon microneedles that mimic the function and dimensions of a mosquito's mouthparts are proposed. Two-step etching and deep reactive ion etching from both sides of the wafer were used to etch the boreholes completely and to ensure the holes have lateral smoothness. Microneedles composed of {411} exterior crystal planes were formed by anisotropic etching in 40% KOH solution at a water-bath temperature of 87°C. Finally, hollow silicon microneedles with a shank height of 100–120 µm and needle borehole diameter of 10–25 µm were fabricated. Flow rate tests using hollow microneedles were performed and demonstrated that the correlation between the flow rate and the inner diameter follows the Hagen-Poiseuille law. Sample tests were performed using pig skin and have shown that the microneedles have sufficient strength to withstand breakup. The microneedles, that the authors fabricated by using the microelectromechanical system, have potential applications in painless transdermal drug delivery systems.

1. Introduction: In the past few decades, the microelectromechanical system (MEMS) and micro total analysis systems have enabled great progress to be made in the field of health and medical welfare. Transdermal drug delivery systems (TDDSs) have played a particularly important role. TDDS is a mechanism that creates a drug flow into the skin and promotes subsequent absorption into the circulation system via blood capillaries [1]. Compared with traditional drug delivery systems, TDDS has several advantages such as avoiding drug decomposition by oral administration and reducing pain and the possibility of infection during intravenous injection. In recent years, using the microneedle arrays to improve skin permeability is a relatively new way for TDDS technology as it can create channels in the micrometre range, allowing complex macromolecules to pass through [2]. The main features of microneedles are accuracy, painlessness, convenience and efficacy of use.

Generally speaking, microneedles were made of silicon, polymer, metal etc. [3–8]. Silicon is the most commonly used material since it has good mechanical and electrical properties. Furthermore, its biocompatibility is superior to metals. Silicon microneedles can also be made in batch using MEMS technology [3, 8]. Anisotropic wet etching is a simple low-cost process to produce microneedles with uniform corrosion rate [7]. Gardeniers *et al.* [8] have previously demonstrated a fabrication method based on the cryogenic reactive ion etching (RIE) process with silicon nitride (Si₃N₄) as a wet etch mask and anisotropic silicon wet etching of the {111} plane bounding the needle structures.

In this Letter, we demonstrate hollow microneedles with heights of 100–120 µm and borehole diameters of 10–25 µm, bound by an etching {411} plane, through a series of experiments of dry etching and anisotropic wet etching. We also carry out fluid injection tests on pig skin with the aid of a syringe pump. We demonstrate that the microneedles have sufficient mechanical strength.

2. Design of hollow microneedles: Stratum corneum in thickness from 5 to 20 µm forms the outermost protective layer of skin. The epidermis, which varies from 20 to 100 µm in thickness, sits between the stratum corneum and dermis. Blood vessels and capillaries lie in the dermis [9]. Consequently, injection will be painless at a depth of 20–100 µm in the epidermis as the needles do not reach the upper nerve cells. The drug, however, is able to diffuse deeper into the skin and is absorbed into the capillary system of the dermis. Therefore the design length of the microneedles is about 100 µm.

Mosquitoes' mouthparts can penetrate human skin to complete blood collection, while the victim is unaware of the process [10, 11].

We propose that the serrated maxillas and the small appearance of mosquito mouthparts can be mimicked in hollow silicon microneedles. The largest inner diameter of the hollow microneedles proposed here is the same as the inner diameter of mosquitoes' mouthparts. To make the needle wall similar to the serrated maxillas, wet etching is chosen to fabricate the needle tips. The needle wall has certain roughness that reduces the contact area with the skin and therefore pain [11].

3. Experimental details: Fig. 1a shows the process flow for the hollow out-of-plane microneedles. Low resistivity (1–10 Ω cm), N-type, double-side-polished silicon wafers with thickness of 350 µm, and {100} crystal orientation, were used as the starting substrate material. Owing to the limit of the maximum etching aspect ratio achievable with the deep RIE (DRIE) tool in our laboratory, etching from both sides of the wafer was performed to etch the boreholes completely and to ensure a hole with a certain degree of lateral smoothness.

A layer of SiO₂ was first deposited on both sides of the wafer by thermal oxidation [Fig. 1a (a)]. A thin layer of a photoresist was then spin-coated and patterned on the backside of the wafer. This step was followed by a SiO₂ etch, to form a hard mask for a subsequent DRIE etch [Fig. 1a (b)]. Patterned holes were then etched into the silicon substrate by DRIE using an inductively coupled plasma (ICP) etcher (ALCATEL AMS100SE). Parameters shown in Table 1 were used for etching the boreholes at the beginning of the dry etching process. The phenomenon of etching stop appeared when the microhole reached a certain depth [12]. Therefore a two-step DRIE process was used for hole etching. First, the parameters in Table 1 were used to etch the silicon for 40 min. Second, the parameters in Table 2 were used for the second etching step in which oxygen gas was introduced, following the same approach as in the first step.

The holes were formed to a total depth of 245 µm [Fig. 1a (c)]. Fig. 1b shows the scanning electron microscope (SEM) profile of 20 µm microholes after the first DRIE from the bottom side of the silicon wafer.

The front-side needle boreholes were defined using a Karl Suss MA/BA6 mask aligner in a thin photoresist (2–3 µm) [Fig. 1a (d)]. These holes were then etched using DRIE until they connected and overlapped with the holes extended from the opposite side, at an approximate depth of 160 µm [Fig. 1a (e)]. Removing the patterned SiO₂ from both sides of the wafer leaves a clean surface for fabrication of the needles. The SEM profile of 20 µm microholes after etching from both sides of the wafer is shown in Fig. 1c.

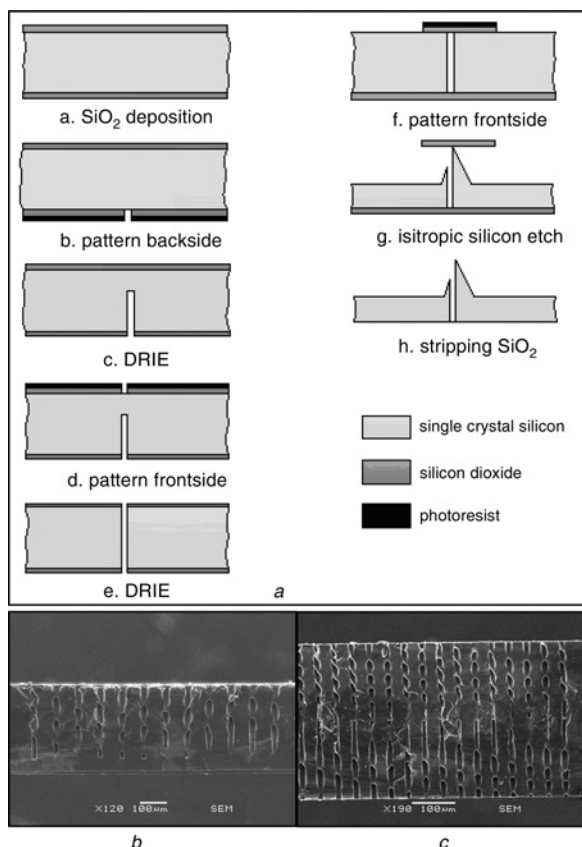


Figure 1 Process flow for hollow out-of-plane microneedles fabrication (Fig. 1a); SEM images of microholes with diameter of 20 μm after DRIE from one side (Fig. 1b); both sides of wafer (Fig. 1c); sample cleaved along $\{100\}$ plane which includes the cross-section of microholes

Table 1 DRIE process conditions of first etching step

Gas	Flow, sccm	Cycle duration, s	Pressure, mBar	Source power, W	Substrate holder power, W
SF ₆	700	7	0.088	2800	80
C ₄ F ₈	220	2	0.032	2800	60

The wafer was coated with SiO₂ again by thermal oxidation. A thin layer of photoresist was spin-coated and patterned on the front side of the wafer [Fig. 1a (f)]. The square mask was used in the wet etching process. The wafer was etched in 40% KOH solution at 87°C to obtain microneedles with a height of 100 μm composed of $\{411\}$ crystal planes [Fig. 1a (g)]. Finally, microneedles with the designed height were obtained [Fig. 1a (h)].

4. Results and discussion: Anisotropic properties of silicon are dependent on the etching rates of individual planes (hkl) and their ratios $V\{h_1k_1l_1\}/V\{h_2k_2l_2\}$ under etching conditions. The final shape of the microneedle is mainly composed by the plane with a slower etching rate rather than the one with a faster etching rate [13]. If the etching rate ratio of $V\{133\}/V\{411\}$ is relatively low, the exterior plane of the needle tends to $\{133\}$. Otherwise, the plane tends to $\{411\}$. If a mask pattern is properly aligned, $\{133\}$ and $\{411\}$ crystal planes can be easily observed during the etching process. The analysis of experimental conditions which have effects on the etching rate ratio of $V\{133\}/V\{411\}$ was studied as follows.

Table 2 DRIE process conditions of second etching step

Gas	Flow, sccm	Cycle duration, s	Pressure, mBar	Source power, W	Substrate holder power, W
SF ₆	700	8	0.093	2800	100
C ₄ F ₈	220	3	0.038	2800	60
O ₂	100	3	0.029	2800	120

4.1. Effects of solution concentration on $V\{133\}/V\{411\}$: The type of the microneedle crystal plane was studied under the condition of a variable etching solution concentration at a constant temperature of 87°C, as shown in the SEM images of Fig. 2. From the experimental results, $\{411\}$ crystal planes account for the major part of the silicon microneedles when the etching solution of 30% KOH was used, however a small quantity of $\{133\}$ crystal planes also appeared. With an increase of the KOH concentration, the microneedles gradually tend to $\{411\}$ crystal planes. When using the etching solution of 50% KOH, the silicon needles were composed mostly of $\{411\}$ planes.

Fig. 2 quantitatively describes the effect of etching solution concentration on the crystal planes of microneedles. With the increase of concentration of KOH solution, the etching rate ratio of $V\{133\}/V\{411\}$ grows larger and the crystal plane of the silicon microneedle tends to $\{411\}$. The etching time for certain heights of silicon needles gradually increases with the increase of KOH solution concentration.

4.2. Effects of mask on etching of silicon microneedles: To investigate the effect of mask size on the formation of 100 μm deep microneedles, gradient graphics were used. Table 3 shows the mask sizes used in the experiments. Microneedles with inclined holes can be produced by moving the centre of the holes with respect to the tip by an offset distance δ . Using this method, hole congestion can be effectively avoided and the wall strength enhanced to prevent needle breakup when inserted into skin. Experiments have revealed that hollow microneedles with various offset distances can be obtained using the designed mask sizes.

Through a series of DRIE and anisotropic wet etching experiments, hollow silicon microneedles with heights of over 100 μm and hole diameters of 10–25 μm were fabricated under the

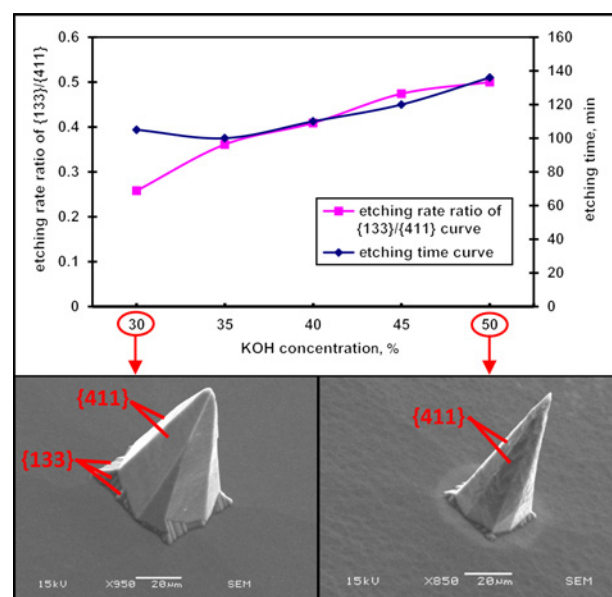
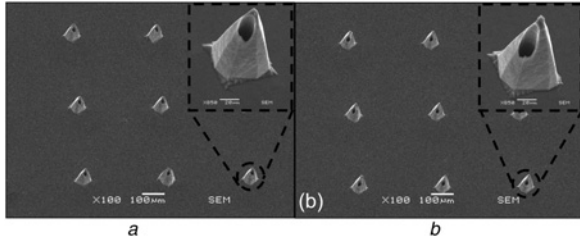


Figure 2 Effect of KOH concentration on etching time and etching rate ratio of the $V\{133\}/V\{411\}$
Etching solution temperature was maintained at 87°C

Table 3 Mask sizes for wet anisotropic etching of silicon microneedles

Mask size in square, μm		Inner diameter of microneedles, μm			
		10	15	20	25
Offset distance δ , μm	5	205	210	215	220
	10	210	215	220	225
	15	215	220	225	230
	20	220	225	230	235

**Figure 3** SEM micrographs of arrays of microneedles with boreholes of 20 μm diameter and offsetsa $\delta = 5 \mu\text{m}$ b $\delta = 10 \mu\text{m}$

Inserted micrographs show magnified needle specimens selected from the arrays

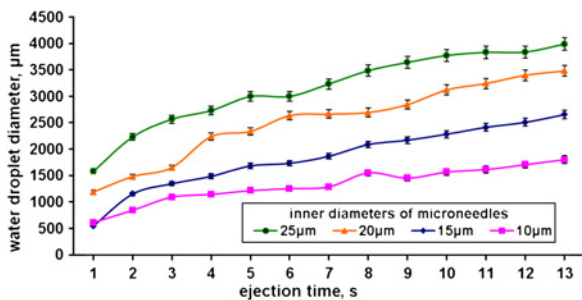
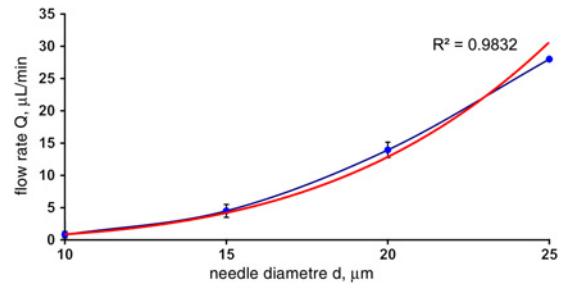
condition of 40% KOH solution and a water-bath temperature of 87°C. In addition, the centre of the microneedles are offset from the tip of the borehole by 5–20 μm . Figs. 3a and b show SEM micrographs of microneedle arrays with boreholes 20 μm in diameter and offsets δ of 5 and 10 μm , respectively. The inserted micrographs show magnified needle specimens selected from each array.

5. Performance evaluation

5.1. Fluidic ejection tests: A liquid supply was provided by bonding the microneedle chips to PDMS substrates containing 3 mm diameter input ports. A syringe pump was used to control the flow rate of deionised (DI) water at 10 $\mu\text{L}/\text{min}$ and the injection pressure. The water droplet diameter at certain ejection times was observed by using a microscope with a high-speed magnified video capture capability. Microneedles with inner diameters of 10, 15, 20, 25 μm were tested to obtain the relationship between water droplet diameter and ejection time, as shown in Fig. 4.

The resulting volumetric flow rate of water ejection was calculated on the basis of variation in the diameter of the water droplet with time. Assuming that the droplet forms a partial sphere, the volume V of the water droplet can be calculated by the following formula [14]

$$V = \frac{\pi}{6} h (3r^2 + h^2) \quad (1)$$

**Figure 4** Time dependence of water droplet diameter for microneedles with inner diameters ranging from 10 to 25 μm **Figure 5** Relationship between flow rate and microneedles' inner diameter

where r and h are the radius and height of the droplet, respectively. In addition, the height h can also be calculated by the following equation: $h = r \tan(\theta/2)$, using a water contact angle θ of 40° on a silicon surface.

Therefore the diameter of the water droplet can be obtained for each second from Fig. 4 and then the droplet volume can be calculated by (1). The flow rate Q , for example, the droplet volume at each ejection second, for needles with different diameters can be then obtained, as shown in Fig. 5.

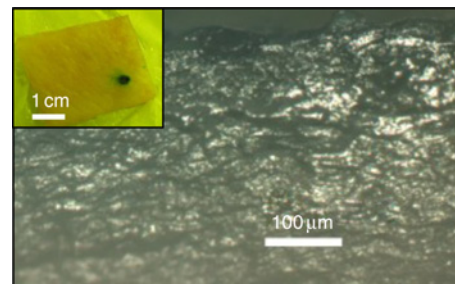
In the Hagen-Poiseuille law, the volumetric flow rate Q is expressed by the following equation [14]

$$Q = \frac{\pi d^4 \Delta P}{128 \eta L} \quad (2)$$

where d (m) is the inner diameter of a cylindrical tube, ΔP (Pa) is the pressure difference between the two ends, η (Pa s) is the viscosity of the fluid and L (m) is the length of the borehole. This equation indicates that the flow rate is proportional to the fourth power of the tube diameter. According to Norihsa *et al.* [14], the ejection pressure should remain constant if the inner diameter of the microneedles is larger than 10 μm . Assuming that this is valid in our experiments, we find the flow rate Q to be proportional to the 3.9th power of the needle diameter and its correlation is as high as $R^2 = 0.98$, suggesting that the experimental results comply with the Hagen-Poiseuille law.

5.2. Pig skin puncture tests: Microneedle arrays were used to inject dyed DI water into pig skin. Pig skin was used in this experiment because of its physiological similarity to human skin. The fresh pig skin was acquired from a local slaughterhouse.

The underlying subcutaneous fat was gently scraped off until the skin was about 2 mm thick. The array of 25 μm ID microneedles was then placed onto the skin sample, and injection was carried out under the control of a syringe pump, as shown in Fig. 6. The inserted picture shows the pig skin with the clearly visible injection point. After DI water injection, the specimen was rested for 5 h so that the fluid could spread to deeper layers of the skin and then frozen for 2 h. The cross-section of the sample at the injection site indicated that the liquid was injected into the skin to a depth

**Figure 6** Photographs of pig skin before and after cutting at the injection site

of at least 100 μm . We found that the microneedles remained intact even after several injection experiments. This indicates that the microneedle array has good endurance and can be used for repetitive transdermal injection.

6. Conclusions: Using a combination of DRIE and anisotropic wet etching, hollow out-of-plane silicon microneedles with a shank height of 100–120 μm and the needle borehole diameter of 10–25 μm have been presented. The dimensions of the needles' borehole are similar to the mouthparts of mosquitoes. The conclusion that the fluid flow follows the Hagen-Poiseuille law has been demonstrated by ejection tests. Using the pig skin model, it has been shown that the needles have good strength and excellent endurance. The roughness of the needle wall obtained by anisotropic wet etching can decrease the contact area of the skin and the needle surface to reduce tissue damage and subsequent pain. The hollow out-of-plane silicon microneedles presented have potential applications in the future for painless TDDS.

7. Acknowledgments: This work is funded under the National Natural Science Foundation of China (Project numbers 51075059, 20890024). The authors are grateful to Ying Zhang and Zheng Xu for their contributions to the work.

8 References

- [1] Nordquist L., Roxhed N., Griss P., Stemme G.: 'Novel microneedle patches for active insulin delivery are efficient in maintaining glycaemic control: an initial comparison with subcutaneous administration', *Pharm. Res.*, 2007, **24**, (7), pp. 1381–1388
- [2] Mark R.: 'Microneedles for transdermal drug delivery', *Adv. Drug Deliv. Rev.*, 2004, **56**, pp. 581–587
- [3] Kim Y.-C., Park J.-H., Prausnitz M.R.: 'Microneedles for drug and vaccine delivery', *Adv. Drug Deliv. Rev.*, 2012, **64**, (14), pp. 1547–1568
- [4] Boris S., Dorian L.: 'Arrays of hollow out-of-plane microneedles for drug delivery', *J. Microelectromech. Syst.*, 2005, **14**, (3), pp. 472–479
- [5] Parker E.R., Rao M.P., Turner K.L., Meinhardt C.D., MacDonald N.C.: 'Bulk micromachined titanium microneedles', *J. Microelectromech. Syst.*, 2007, **16**, (2), pp. 289–295
- [6] Park J.H., Allen M.G., Prausnitz M.R.: 'Biodegradable polymer microneedles: fabrication, mechanics and transdermal drug delivery', *J. Control Release*, 2005, **104**, pp. 51–66
- [7] Wilke N., Mulcahy A., Ye S.-R., Morrissey A.: 'Process optimization and characterization of silicon microneedles fabricated by wet etch technology', *Microelectron. J.*, 2005, **36**, pp. 650–656
- [8] Gardeniers H.J.G.E., Luttge R., Berenschot E.J.W., *ET AL.*: 'Silicon micromachined hollow microneedles for transdermal liquid transport', *J. Microelectromech. Syst.*, 2003, **12**, (6), pp. 855–862
- [9] Bangtao C., Jiashen W., Ciprian I.: 'Sonophoretic enhanced microneedles array (SEMA) – Improving the efficiency of transdermal drug delivery', *Sens. Actuators B*, 2010, **145**, pp. 54–60
- [10] Jingchun W.: 'Coupling bionic research on painless injector needles based on insect piercing-sucking mouthpart'. PhD. thesis, Jilin University, People's Republic of China, 2008
- [11] Izumi H., Suzuki M., Aoyagi S., Kanzaki T.: 'Realistic imitation of mosquito's proboscis: electrochemically etched sharp and jagged needles and their cooperative inserting motion', *Sens. Actuators A*, 2011, **165**, pp. 115–123
- [12] Abdolvand R., Ayazi F.: 'An advanced reactive ion etching process for very high aspect-ratio sub-micron wide trenches in silicon', *Sens. Actuators A*, 2008, **144**, pp. 109–116
- [13] Zubel I., Barycka I.: 'Silicon anisotropic etching alkaline solutions I: the geometric description of figures developed under etching Si (100) in various solutions', *Sens. Actuators A*, 1998, **70**, pp. 250–259
- [14] Norihisa K., Ryotaro O., Takahiro S., *ET AL.*: 'Experimental and computational analysis of water-droplet formation and ejection process using hollow microneedle', *Jpn. J. Appl. Phys.*, 2011, **50**, p. 067202